Lecture notes on topological insulators

Ming-Che Chang

Department of Physics, National Taiwan Normal University, Taipei, Taiwan

(Dated: December 2, 2024)

CONTENTS

I. TWO-DIMENSIONAL MATERIAL

A. Graphene

A graphene lattice is a honeycomb (or hexagonal) lattice that consists of two triangular lattices (Fig. 1). We will call them sublattice-A and sublattice-B. Write the basis vectors of lattice-A as $\mathbf{a}_1$ and $\mathbf{a}_2$, then a general lattice vector

$$\mathbf{R} = n_1\mathbf{a}_1 + n_2\mathbf{a}_2,\ n_1, n_2 \in Z. \tag{1.1}$$

For convenience, we will have an extra vector $\mathbf{a}_3$ such that (see Fig. 1(a))

$$\mathbf{a}_1 = \sqrt{3}a\hat{x}, \tag{1.2}$$
$$\mathbf{a}_2 = -\frac{\sqrt{3}}{2}a\hat{x} + \frac{3}{2}a\hat{y}, \tag{1.3}$$
$$\mathbf{a}_3 = -\frac{\sqrt{3}}{2}a\hat{x} - \frac{3}{2}a\hat{y}. \tag{1.4}$$

Note that $a_0 = \sqrt{3}a \simeq 2.46\mathring{A}$ is the lattice constant of graphene. From basis vector $\mathbf{a}_1$ and $\mathbf{a}_2$, we have the basis vectors for the reciprocal lattice (see Fig. 1(b)),

$$\mathbf{b}_1 = \frac{2\pi}{a}\left(\frac{1}{\sqrt{3}}\hat{x} + \frac{1}{3}\hat{y}\right), \tag{1.5}$$
$$\mathbf{b}_2 = \frac{2\pi}{a}\frac{2}{3}\hat{y}. \tag{1.6}$$

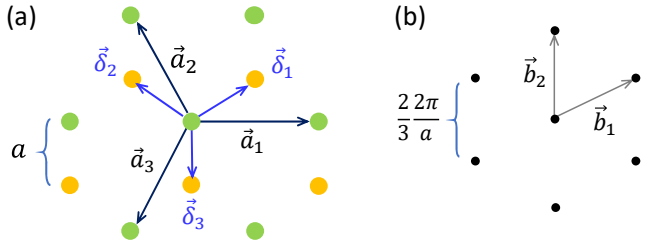

FIG. 1 (a) A graphene lattice consists of two triangular lattices: sublattice-A (green dots) and -B (orange dots). (b) Reciprocal lattice of sublattice-A.

Furthermore, choose the displacement vectors:

$$\boldsymbol{\delta}_1 = \frac{\sqrt{3}}{2}a\hat{x} + \frac{1}{2}a\hat{y}, \tag{1.7}$$
$$\boldsymbol{\delta}_2 = -\frac{\sqrt{3}}{2}a\hat{x} + \frac{1}{2}a\hat{y}, \tag{1.8}$$
$$\boldsymbol{\delta}_3 = -a\hat{y}. \tag{1.9}$$

For graphene, sublattice-A is displaced by $\boldsymbol{\delta}_i$ with respect to sublattice-B. A general lattice vector for sublattice-B can be written as $\mathbf{R} + \boldsymbol{\delta}_1$.

Suppose electron spin can be ignored. Write the creation and annihilation operators for sublattice-A and -B as $c^\dagger_{\mathbf{R}}, c_{\mathbf{R}}$ and $d^\dagger_{\mathbf{R}+\boldsymbol{\delta}_1}, d_{\mathbf{R}+\boldsymbol{\delta}_1}$, then the tight-binding Hamiltonian for graphene is

$$\hat{H} = \hat{H}_{NN} + \hat{H}_{NNN} + \hat{H}_{on-site}. \tag{1.10}$$

We have included only the nearest-neighbor (NN) hoppings between A-B sublattcies, the next-nearest-neighbor (NNN) hoppings among A (or B) sublattice, and the on-site interactions:

$$\hat{H}_{NN} = t_1 \sum_{\mathbf{R}} \left(d^\dagger_{\mathbf{R}+\boldsymbol{\delta}_1} c_{\mathbf{R}} + d^\dagger_{\mathbf{R}+\boldsymbol{\delta}_2} c_{\mathbf{R}} + d^\dagger_{\mathbf{R}+\boldsymbol{\delta}_3} c_{\mathbf{R}} \right) + h.c.,$$

$$\begin{aligned}\hat{H}_{NNN} &= t_2 \sum_{\mathbf{R}} \left(c^\dagger_{\mathbf{R}+\mathbf{a}_1} c_{\mathbf{R}} + c^\dagger_{\mathbf{R}+\mathbf{a}_2} c_{\mathbf{R}} + c^\dagger_{\mathbf{R}+\mathbf{a}_3} c_{\mathbf{R}} \right) \\ &+ t_2 \sum_{\mathbf{R}} \left(d^\dagger_{\mathbf{R}+\boldsymbol{\delta}_1+\mathbf{a}_1} d_{\mathbf{R}+\boldsymbol{\delta}_1} + d^\dagger_{\mathbf{R}+\boldsymbol{\delta}_1+\mathbf{a}_2} d_{\mathbf{R}+\boldsymbol{\delta}_1} \right. \\ &\left. + d^\dagger_{\mathbf{R}+\boldsymbol{\delta}_1+\mathbf{a}_3} d_{\mathbf{R}+\boldsymbol{\delta}_1} \right) + h.c.,\end{aligned} \tag{1.11}$$

and

$$\hat{H}_{on-site} = \Delta \sum_{\mathbf{R}} c^\dagger_{\mathbf{R}} c_{\mathbf{R}} - \Delta \sum_{\mathbf{R}} d^\dagger_{\mathbf{R}+\boldsymbol{\delta}_1} d_{\mathbf{R}+\boldsymbol{\delta}_1},$$

in which t_1, t_2 are hopping amplitudes, and $2\Delta(\geq 0)$ is the difference of on-site energies between two sublattices. The hopping amplitudes are assumed to be real-valued for simplicity.

Impose the periodic boundary condition on the graphene sheet, then the system has translation symmetry and we can rely on Fourier transformation to diagonalize the Hamiltonian. Write

$$c_{\mathbf{R}} = \frac{1}{\sqrt{N}} \sum_{\mathbf{k}} e^{i\mathbf{k}\cdot\mathbf{R}} c_{\mathbf{k}}, \tag{1.12}$$

$$\text{or } c_{\mathbf{k}} = \frac{1}{\sqrt{N}} \sum_{\mathbf{R}} e^{-i\mathbf{k}\cdot\mathbf{R}} c_{\mathbf{R}}, \tag{1.13}$$

in which N is the total number of lattice points in one sublattice, and

$$d_{\mathbf{R}+\boldsymbol{\delta}_1} = \frac{1}{\sqrt{N}} \sum_{\mathbf{k}} e^{i\mathbf{k}\cdot(\mathbf{R}+\boldsymbol{\delta}_1)} d_{\mathbf{k}}, \tag{1.14}$$

$$\text{or } d_{\mathbf{k}} = \frac{1}{\sqrt{N}} \sum_{\mathbf{R}} e^{-i\mathbf{k}\cdot(\mathbf{R}+\boldsymbol{\delta}_1)} d_{\mathbf{R}+\boldsymbol{\delta}_1}. \tag{1.15}$$

With the Fourier transformation, one has, for example,

$$\begin{aligned} \sum_{\mathbf{R}} d^\dagger_{\mathbf{R}+\boldsymbol{\delta}_1} c_{\mathbf{R}} &= \frac{1}{N} \sum_{\mathbf{k},\mathbf{k}'} \sum_{\mathbf{R}} e^{-i(\mathbf{k}'-\mathbf{k})\cdot\mathbf{R}} e^{-i\mathbf{k}'\cdot\boldsymbol{\delta}_1} d^\dagger_{\mathbf{k}'} c_{\mathbf{k}} \\ &= \sum_{\mathbf{k}} e^{-i\mathbf{k}\cdot\boldsymbol{\delta}_1} d^\dagger_{\mathbf{k}} c_{\mathbf{k}}, \end{aligned} \tag{1.16}$$

in which the orthogonality relation has been used,

$$\sum_{\mathbf{R}} e^{i(\mathbf{k}'-\mathbf{k})\cdot\mathbf{R}} = N\delta_{\mathbf{k}'\mathbf{k}}. \tag{1.17}$$

After some more calculations, we have

$$\begin{aligned} \hat{H} &= t_1 \sum_{\mathbf{k}} \left(e^{-i\mathbf{k}\cdot\boldsymbol{\delta}_1} + e^{-i\mathbf{k}\cdot\boldsymbol{\delta}_2} + e^{-i\mathbf{k}\cdot\boldsymbol{\delta}_3}\right) d^\dagger_{\mathbf{k}} c_{\mathbf{k}} \\ &+ t_2 \sum_{\mathbf{k}} \left(e^{-i\mathbf{k}\cdot\mathbf{a}_1} + e^{-i\mathbf{k}\cdot\mathbf{a}_2} + e^{-i\mathbf{k}\cdot\mathbf{a}_3}\right) c^\dagger_{\mathbf{k}} c_{\mathbf{k}} \\ &+ t_2 \sum_{\mathbf{k}} \left(e^{-i\mathbf{k}\cdot\mathbf{a}_1} + e^{-i\mathbf{k}\cdot\mathbf{a}_2} + e^{-i\mathbf{k}\cdot\mathbf{a}_3}\right) d^\dagger_{\mathbf{k}} d_{\mathbf{k}} + h.c. \\ &+ \Delta \sum_{\mathbf{k}} \left(c^\dagger_{\mathbf{k}} c_{\mathbf{k}} - d^\dagger_{\mathbf{k}} d_{\mathbf{k}}\right) \end{aligned} \tag{1.18}$$

$$= \sum_{\mathbf{k}} \left(c^\dagger_{\mathbf{k}}, d^\dagger_{\mathbf{k}}\right) \mathsf{H}(\mathbf{k}) \begin{pmatrix} c_{\mathbf{k}} \\ d_{\mathbf{k}} \end{pmatrix}. \tag{1.19}$$

For each momentum $\mathbf{k}$, we have an independent subsystem described by a 2×2 matrix,

$$\begin{aligned} \mathsf{H}(\mathbf{k}) &= \begin{pmatrix} 2t_2 \sum_i \cos\mathbf{k}\cdot\mathbf{a}_i + \Delta & t_1 \sum_i e^{i\mathbf{k}\cdot\boldsymbol{\delta}_i} \\ t_1 \sum_i e^{-i\mathbf{k}\cdot\boldsymbol{\delta}_i} & 2t_2 \sum_i \cos\mathbf{k}\cdot\mathbf{a}_i - \Delta \end{pmatrix} \\ &= h_0(\mathbf{k}) + \mathbf{h}(\mathbf{k})\cdot\boldsymbol{\sigma}, \end{aligned} \tag{1.20}$$

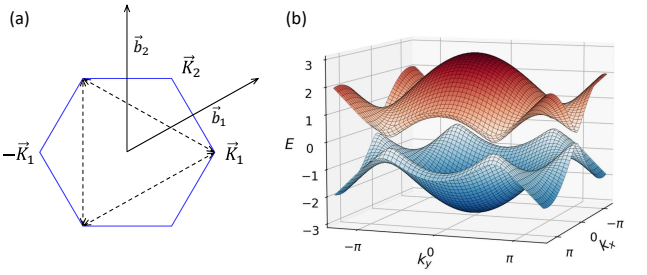

FIG. 2 (a) The Brillouin zone of graphene. The corner points differ by reciprocal lattice vectors are considered equivalent. Hence, the 3 points connected by dotted lines are equivalent to point-$\mathbf{K}_1$, while the other three are equivalent to point $\mathbf{K}_2$. (b) The conduction band and valence band in the two-band graphene model ($t_1 = 1, t_2 = 0, \Delta = 0.2$). Fig. from online course on topology in condensed matter, Delft Univ.

where

$$h_0(\mathbf{k}) = 2t_2 \sum_i \cos\mathbf{k}\cdot\mathbf{a}_i, \tag{1.21}$$

$$\mathbf{h}(\mathbf{k}) = \left(t_1 \sum_i \cos\mathbf{k}\cdot\boldsymbol{\delta}_i, -t_1 \sum_i \sin\mathbf{k}\cdot\boldsymbol{\delta}_i, \Delta\right). \tag{1.22}$$

The eigen-energies for the subsystem $\mathsf{H}(\mathbf{k})$ are

$$\varepsilon_\pm(\mathbf{k}) = h_0(\mathbf{k}) \pm |\mathbf{h}(\mathbf{k})|, \tag{1.23}$$

where

$$\begin{aligned} |\mathbf{h}| &= \sqrt{3t_1^2 + 2t_1^2 \left(\cos\mathbf{k}\cdot\mathbf{a}_1 + \cos\mathbf{k}\cdot\mathbf{a}_2 + \cos\mathbf{k}\cdot\mathbf{a}_3\right) + \Delta^2} \\ &= \sqrt{3t_1^2 + 2t_1^2 f(\mathbf{k}) + \Delta^2}, \end{aligned} \tag{1.24}$$

in which we have used

$$\boldsymbol{\delta}_1 - \boldsymbol{\delta}_2 = \mathbf{a}_1, \boldsymbol{\delta}_2 - \boldsymbol{\delta}_3 = \mathbf{a}_2, \text{and } \boldsymbol{\delta}_3 - \boldsymbol{\delta}_1 = \mathbf{a}_3. \tag{1.25}$$

Substitute in the values of $\mathbf{a}_i$, we then have

$$f(\mathbf{k}) \equiv \cos\mathbf{k}\cdot\mathbf{a}_1 + \cos\mathbf{k}\cdot\mathbf{a}_2 + \cos\mathbf{k}\cdot\mathbf{a}_3 \tag{1.26}$$

$$= \cos\sqrt{3}ak_x + 2\cos\frac{\sqrt{3}}{2}ak_x \cos\frac{3}{2}ak_y. \tag{1.27}$$

When plotted, the conduction band and the valence band are separated by an energy gap 2Δ (Fig. 2) at the corners of the hexagonal Brillouin zone called Dirac points.

1. Symmetries

A graphene Hamiltonian could have the following symmetries:

1. Time-reversal symmetry (TRS),

$$\mathsf{H}^*(-\mathbf{k}) = \mathsf{H}(\mathbf{k}). \tag{1.28}$$

This gives

$$h_x(-\mathbf{k}) = h_x(\mathbf{k}),\ h_y(-\mathbf{k}) = -h_y(\mathbf{k}),\ h_z(-\mathbf{k}) = h_z(\mathbf{k}). \tag{1.29}$$

2. Space-inversion symmetry (SIS) with respect to the center of a hexagon,

$$\sigma_x \mathsf{H}(-\mathbf{k})\sigma_x = \mathsf{H}(\mathbf{k}). \tag{1.30}$$

This gives

$$h_x(-\mathbf{k}) = h_x(\mathbf{k}),\ h_y(-\mathbf{k}) = -h_y(\mathbf{k}),\ h_z(-\mathbf{k}) = -h_z(\mathbf{k}). \tag{1.31}$$

If both symmetries exist, then $h_z(=\Delta$ here) must be zero. Conversely, the energy gap 2Δ can be opened when either TRS or SIS is broken.

3. C_3 symmetry around the z-axis passing through the center of a hexagon,

$$\mathsf{H}(\mathsf{R}_{2\pi/3}\mathbf{k}) = \mathsf{H}(\mathbf{k}), \tag{1.32}$$

where $\mathsf{R}_{2\pi/3}$ is the rotation matrix around the z-axis. If $\Delta = 0$, then there is also a reflection symmetry with respect to a mirror plane perpendicular to the graphene plane that passes through the midpoint of a carbon-carbon bond.

In addition to Δ being zero, if t_2 is also zero (i.e. electrons hop only *between* A, B sublattices), then $\mathsf{H}(\mathbf{k})$ does not have diagonal matrix elements, and we have

4. Chiral symmetry (aka Sublattice symmetry),

$$\{\mathsf{H}, \sigma_z\} = 0. \tag{1.33}$$

This leads to

$$\varepsilon_-(\mathbf{k}) = -\varepsilon_+(\mathbf{k}). \tag{1.34}$$

That is, the energy eigenvalues would appear in pairs with opposite energies. However, this is not an exact symmetry of real graphene.

Before moving on, there is a subtle point regarding the Hamiltonian $\mathsf{H}(\mathbf{k})$ (Cayssol and Fuchs, 2021): It is not invariant under the reciprocal lattice translation, $\mathbf{k} \to \mathbf{k} + \mathbf{b}_{1,2}$. If, for sublattice-B, we write $\mathbf{d}_{\mathbf{R}}$ instead of $\mathbf{d}_{\mathbf{R}+\boldsymbol{\delta}_1}$, then

$$d_{\mathbf{R}+\boldsymbol{\delta}_2} \to d_{\mathbf{R}+\boldsymbol{\delta}_2-\boldsymbol{\delta}_1},\ d_{\mathbf{R}+\boldsymbol{\delta}_3} \to d_{\mathbf{R}+\boldsymbol{\delta}_3-\boldsymbol{\delta}_1}. \tag{1.35}$$

The Hamiltonian in Eq. (1.20) becomes

$$\begin{aligned} \mathsf{H}'(\mathbf{k}) &= \begin{pmatrix} 2t_2\sum_i \cos\mathbf{k}\cdot\mathbf{a}_i + \Delta & t_1\sum_i e^{i\mathbf{k}\cdot(\boldsymbol{\delta}_i-\boldsymbol{\delta}_1)} \\ t_1\sum_i e^{-i\mathbf{k}\cdot(\boldsymbol{\delta}_i-\boldsymbol{\delta}_1)} & 2t_2\sum_i \cos\mathbf{k}\cdot\mathbf{a}_i - \Delta \end{pmatrix} \\ &= \mathsf{U}\mathsf{H}(\mathbf{k})\mathsf{U}^\dagger, \end{aligned} \tag{1.36}$$

where

$$\mathsf{U} = \begin{pmatrix} 1 & 0 \\ 0 & e^{i\mathbf{k}\cdot\boldsymbol{\delta}_1}. \end{pmatrix} \tag{1.37}$$

The off-diagonal matrix elements of H' now depend on $\mathbf{a}_2, \mathbf{a}_3$ because of Eq. (1.25). Hence, H' is invariant under the reciprocal lattice translation, $\mathbf{k} \to \mathbf{k} + \mathbf{b}_{1,2}$. It differs from H by a gauge transformation U.

2. Effective Hamiltonian near Dirac point

The gradient of the f in Eq. (1.27) vanishes, $\nabla f = 0$, when

$$\begin{aligned} \sin\sqrt{3}ak_x + \sin\frac{\sqrt{3}}{2}ak_x \cos\frac{3}{2}ak_y &= 0, & (1.38)\\ \sin\frac{3}{2}ak_y &= 0. & (1.39) \end{aligned}$$

The second equation gives $k_y = 0$ or $1/3(2\pi/a)$, and $\cos\frac{3}{2}ak_y = 1$ or -1. Solving for k_x, we then find out the extrema of energy bands at two Dirac points and their equivalent points (Fig. 2)

$$\begin{aligned} \mathbf{K}_1 &= \frac{2\pi}{a}\left(\frac{2}{3\sqrt{3}}, 0\right), & (1.40)\\ \mathbf{K}_2 &= \frac{2\pi}{a}\left(\frac{1}{3\sqrt{3}}, \frac{1}{3}\right) & (1.41) \end{aligned}$$

One can also pick $\mathbf{K}_1$ and $\mathbf{K}_2 = -\mathbf{K}_1$ as two inequivalent Dirac points. It follows that $f(\mathbf{K}_1) = f(\mathbf{K}_2) = -\frac{3}{2}$, $|\mathbf{h}(\mathbf{K}_{1,2})| = \Delta$, and the energy gap at Dirac points $\Delta\varepsilon = 2\Delta$.

Next, consider the momenta near the Dirac points,

$$\mathbf{k} = \mathbf{K}_i + \mathbf{k}_i, \quad |\mathbf{k}_i| \ll |\mathbf{K}_i|;\ i = 1, 2. \tag{1.42}$$

Expand the momenta in Hamiltonian $\mathsf{H}(\mathbf{k})$ with respect to $\mathbf{K}_{1,2}$, keep the terms linear in $\mathbf{k}_{1,2}$ and ignore higher-order terms. Then the diagonal matrix elements H_{11} and H_{22} are simply $6t_2 \pm \Delta$. The off-diagonal matrix elements near $\mathbf{K}_i$ are,

$$H_{12}(\mathbf{k}) = t_1\left(e^{i\mathbf{K}_i\cdot\boldsymbol{\delta}_1}e^{i\mathbf{k}_i\cdot\boldsymbol{\delta}_1} + e^{i\mathbf{K}_i\cdot\boldsymbol{\delta}_2}e^{i\mathbf{k}_i\cdot\boldsymbol{\delta}_2} + e^{i\mathbf{K}_i\cdot\boldsymbol{\delta}_3}e^{i\mathbf{k}_i\cdot\boldsymbol{\delta}_3}\right). \tag{1.43}$$

From the table below (choose $\mathbf{K}_2 = -\mathbf{K}_1$),

	$i=1$	2	3
$\mathbf{K}_1\cdot\boldsymbol{\delta}_i =$	$+\frac{2\pi}{3}$	$-\frac{2\pi}{3}$	0
$\mathbf{K}_2\cdot\boldsymbol{\delta}_i =$	$-\frac{2\pi}{3}$	$+\frac{2\pi}{3}$	0
$e^{i\mathbf{K}_{1/2}\cdot\boldsymbol{\delta}_i} =$	$-\frac{1}{2}\mp\frac{\sqrt{3}}{2}i$	$-\frac{1}{2}\pm\frac{\sqrt{3}}{2}i$	1

(1.44)

we have ($\mathbf{k}_i$ are now simply written as $\mathbf{k}$)

$$\begin{aligned} H_{12}(\mathbf{k}) &\simeq it_1a\mathbf{k}\cdot\left(\mp\frac{3}{2}i, -\frac{3}{2}\right) & (1.45)\\ &= t_1a\left(\pm\frac{3}{2}k_x - \frac{3}{2}ik_y\right). & (1.46) \end{aligned}$$

Thus, apart from a constant,

$$\begin{aligned} \mathsf{H}(\mathbf{k}) &\simeq \begin{pmatrix} \Delta & \frac{3}{2}t_1a(\pm k_x - ik_y) \\ \frac{3}{2}t_1a(\pm k_x + ik_y) & -\Delta \end{pmatrix} \\ &= \hbar v_F(\tau k_x\sigma_x + k_y\sigma_y) + \Delta\sigma_z, \end{aligned} \tag{1.47}$$

where $\hbar v_F \equiv \frac{3}{2}t_1a$, and $\tau = \pm$ for the states near $\mathbf{K}_{1/2}$.

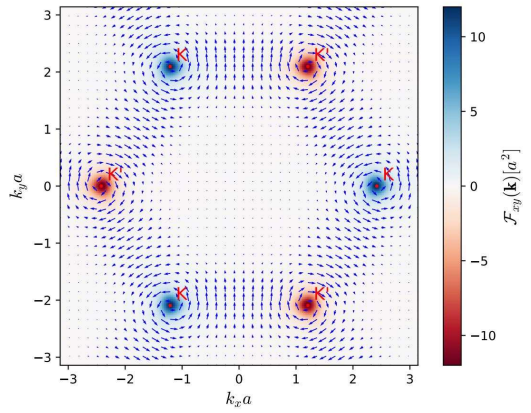

FIG. 3 Distributions of Berry connection (vectors) and Berry curvature (color) in a Brillouin zone. Fig. from J. Atteia's thesis, 2018

3. Berry curvature

Given a two-band Hamiltonian,

$$\mathsf{H}(\mathbf{k}) = h_0(\mathbf{k}) + \mathbf{h}(\mathbf{k})\cdot\boldsymbol{\sigma}, \tag{1.48}$$

the Berry curvature of its electronic states would be

$$F_z^{\pm}(\mathbf{k}) = \mp\frac{1}{2h^3}\mathbf{h}\cdot\frac{\partial\mathbf{h}}{\partial k_x}\times\frac{\partial\mathbf{h}}{\partial k_y}. \tag{1.49}$$

Starting from the $\mathbf{h}$ vector in Eq. (1.22), one gets

$$\begin{aligned}\frac{\partial\mathbf{h}}{\partial k_x} &= \left(-t_1\sum\sin(\mathbf{k}\cdot\boldsymbol{\delta}_i)\delta_{ix}, -t_1\sum\cos(\mathbf{k}\cdot\boldsymbol{\delta}_i)\delta_{ix}, 0\right),\\ \frac{\partial\mathbf{h}}{\partial k_y} &= \left(-t_1\sum\sin(\mathbf{k}\cdot\boldsymbol{\delta}_i)\delta_{iy}, -t_1\sum\cos(\mathbf{k}\cdot\boldsymbol{\delta}_i)\delta_{iy}, 0\right).\end{aligned}$$

After some calculations, it follows that

$$F_z^{\pm}(\mathbf{k}) = \mp\frac{\sqrt{3}/2}{2h^3}a^2t_1^2\Delta\left(\sin\mathbf{k}\cdot\mathbf{a}_1 + \sin\mathbf{k}\cdot\mathbf{a}_2 + \sin\mathbf{k}\cdot\mathbf{a}_3\right), \tag{1.50}$$

in which h can be found in Eq. (1.24). Note that $F_z^{\pm}(\mathbf{k})$ has the periodicity of the Brillouin zone (Fig. 3).

Near the Dirac points $\tau\mathbf{K}_1(\tau=\pm)$, the Berry curvatures are

$$F_{z\tau}^{\pm}(\mathbf{k}) = \pm\tau\frac{9}{8}\frac{a^2t_1^2\Delta}{h^3} = \pm\tau\frac{1}{2}\frac{\hbar^2v_F^2\Delta}{h^3}, \tag{1.51}$$

where $\hbar v_F = \frac{3}{2}t_1a$. For electrons in the valence band near the $\pm\mathbf{K}$-valleys,

$$F_{z\pm}^{-}(\mathbf{k}) = \pm\frac{1}{2}\frac{\hbar^2v_F^2\Delta}{\left(\hbar^2v_F^2k^2+\Delta^2\right)^{3/2}}. \tag{1.52}$$

The Hall conductivity from a filled valence band is zero because of the cancellation from two valleys.

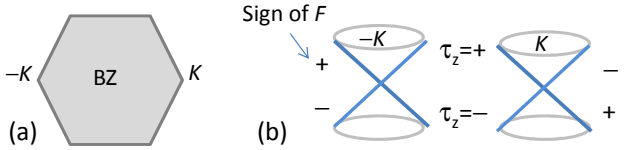

FIG. 4 (a) Brillouin zone of graphene, with valleys K and $-K$. (b) Dirac cones at the two valleys. Valence band has $\tau_z=-$, and conduction band has $\tau_z=+$. The signs of the Berry curvatures for the conduction bands and the valence bands are indicated.

Note that the low-energy Hamiltonians in Eq. (1.47) for the electrons in $\mathbf{K}_1$ and $-\mathbf{K}_1$ valleys are time-reversal conjugate to each other,

$$\mathsf{H}_{-\mathbf{K}}(\mathbf{k}) = \mathsf{H}_{\mathbf{K}}^{*}(-\mathbf{k}). \tag{1.53}$$

Therefore, the Berry curvatures (as well as orbital magnetizations) of the two valleys have opposite signs.

It is left as an exercise to show that the Berry connections near the Dirac points are,

$$A_x^{\pm}(\mathbf{k}) = \frac{\tau}{2}\left(1-\frac{\Delta}{\sqrt{\ }}\right)\frac{\pm k_y}{k^2}, \tag{1.54}$$

$$A_y^{\pm}(\mathbf{k}) = \frac{\tau}{2}\left(1-\frac{\Delta}{\sqrt{\ }}\right)\frac{\mp k_x}{k^2}, \tag{1.55}$$

where

$$\sqrt{\ } \equiv \sqrt{\hbar^2v_F^2k^2+\Delta^2}, \tag{1.56}$$

$$\text{and}\quad N \equiv \left[2\sqrt{\ }\left(\sqrt{\ }+\Delta\right)\right]^{-1/2}. \tag{1.57}$$

4. Degenerate case

In the gapless case with $\Delta=0$, the effective Hamiltonians near the nodes is

$$\mathsf{H}_0 = \hbar v_F\left(\pm k_x\sigma_x + k_y\sigma_y\right), \quad \text{at } \pm K \tag{1.58}$$

$$= \mathbf{h}(\mathbf{k})\cdot\boldsymbol{\sigma}, \tag{1.59}$$

where $\mathbf{h}(\mathbf{k}) = \alpha(\pm k_x, k_y, 0)$. The spins of the electron eigenstates on the Fermi circles are either parallel or anti-parallel to the field $\mathbf{h}(\mathbf{k})$. Therefore, after circling the Fermi circle once, an electron acquires a Berry phase proportional to the solid angle Ω_C extended by the spin vector,

$$\gamma_{\pm} = \mp\frac{1}{2}\Omega_C. \tag{1.60}$$

Since the spin always lies on a plane, the solid angle is 2π, and the Berry phases are $\gamma_{\pm} = \mp\pi$.

Note that the value of the Berry phase $\gamma_C = \pi$ is restricted by time-reversal symmetry: If the electron circles in the opposite direction $-C$, then the Berry phase

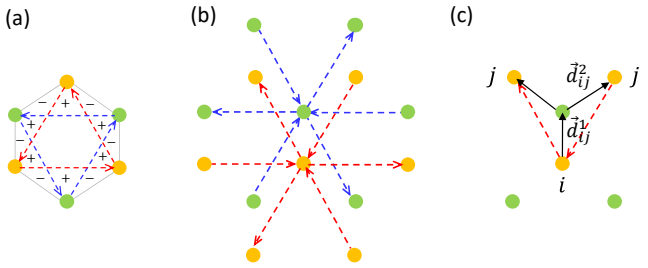

FIG. 5 (a) The alternating flux distribution in the Haldane model. (b) The distribution in (a) can be implemented by alternating phases associated with NNN hoppings. (c) A NNN hopping consisted of two NN hoppings, $\mathbf{d}^1_{ij}$ followed by $\mathbf{d}^2_{ij}$.

becomes $-\gamma_c$. As a result, we should have $\gamma_c = -\gamma_c$ mod 2π. Therefore, γ_c can only be 0 or π.

Due to the phase shift of π for a closed path, one expects to see **weak anti-localization**, instead of **weak localization**, in a graphene or a TI surface with disorders (He *et al.*, 2011). However, real samples are more complicated. Depending on condition, both types of localization can be observed (Lu and Shen, 2014; Tikhonenko *et al.*, 2009).

The value of the Berry phase remains to be π, irrespective of the size of the Fermi circle, as long as the path C encloses the nodal point. This implies that the Berry curvature is a delta function,

$$F^-_{z\pm} = \pm\pi\delta^2(\mathbf{k}). \tag{1.61}$$

This is consistent with the $\Delta \to 0$ limit of Eq. (1.51).

Not only that the two orbitals have opposite monopole charges, the Berry curvatures of the two nodes also have opposite signs, see Fig. 4(b). As a result, the Hall conductivity is zero in the absence of magnetic field.

The Berry curvature of the Dirac point has an effect on the position of energy levels in magnetic field. In a magnetic field perpendicular to the graphene sheet, an electron would circle around the Dirac cone and have the Berry phase of π. According to the **Onsager quantization rule** (Chang and Niu, 1996),

$$\oint_C \mathbf{k}\cdot d\mathbf{r} = 2\pi\left(n + \frac{1}{2} - \frac{\gamma_C}{2\pi}\right). \tag{1.62}$$

The Berry phase term cancels with the 1/2, so that there is no zero-point energy for Landau levels, $\varepsilon_n = v_F\sqrt{2eB\hbar n}$. See Sec. VII.C of Xiao *et al.*, 2010 for a semiclassical derivation of the energy levels. A direct measurement of the Berry phase π from a Dirac point in cold atoms is reported in Duca *et al.*, 2015.

B. Haldane model

1. Haldane flux

The pristine graphene model considered above is topologically trivial. Haldane added a spatially alternating magnetic field to graphene (Fig. 5(a)) so that the electronic states could become topologically nontrivial (Haldane, 1988). To implement this, the phase associated with electron hopping is designed in the following way (Fig. 5(b)):

$$\begin{aligned}
\mathbf{R}_A &\to \mathbf{R}_A + \mathbf{a}_i \text{ get } e^{-i\phi},\ i = 1,2,3 && (1.63)\\
\mathbf{R}_A &\to \mathbf{R}_A - \mathbf{a}_i \text{ get } e^{+i\phi}, && (1.64)\\
\mathbf{R}_B &\to \mathbf{R}_A + \mathbf{a}_i \text{ get } e^{+i\phi}, && (1.65)\\
\mathbf{R}_B &\to \mathbf{R}_A - \mathbf{a}_i \text{ get } e^{-i\phi}. && (1.66)
\end{aligned}$$

As a result, the NNN hoppings between sites i, j among sublattice-A (or -B) become

$$\hat{H}_{NNN} = t_2 \sum_{\ll i,j \gg} e^{i\nu_{ij}\phi} c^\dagger_i c_j, \tag{1.67}$$

where (see Fig. 5(c))

$$\nu_{ij} \equiv \mathrm{sgn}\left(\mathbf{d}^1_{ij} \times \mathbf{d}^2_{ij}\right)_z. \tag{1.68}$$

That is,

$$\begin{aligned}
\hat{H}_{NNN} &= t_2 \sum_{\mathbf{R}} \sum_{i=1}^{3} \left(c^\dagger_{\mathbf{R}+\mathbf{a}_i} c_{\mathbf{R}} e^{-i\phi} + h.c. \right) \\
&+ t_2 \sum_{\mathbf{R}} \sum_{i=1}^{3} \left(d^\dagger_{\mathbf{R}+\mathbf{a}_i} d_{\mathbf{R}} e^{+i\phi} + h.c. \right). && (1.69)
\end{aligned}$$

After Fourier transformation, we have, e.g.,

$$\sum_{\mathbf{R}} c^\dagger_{\mathbf{R}+\mathbf{a}_i} c_{\mathbf{R}} e^{-i\phi} = \sum_{\mathbf{k}} e^{-i\mathbf{k}\cdot\mathbf{a}_i} e^{-i\phi} c^\dagger_{\mathbf{k}} c_{\mathbf{k}}. \tag{1.70}$$

After some calculations, we have

$$\begin{aligned}
&\hat{H}_{NNN} \\
&= 2t_2 \sum_{\mathbf{k}} \sum_i \left[\cos(\mathbf{k}\cdot\mathbf{a}_i + \phi) c^\dagger_{\mathbf{k}} c_{\mathbf{k}} + \cos(\mathbf{k}\cdot\mathbf{a}_i - \phi) d^\dagger_{\mathbf{k}} d_{\mathbf{k}} \right] \\
&= \sum_{\mathbf{k}} \left(c^\dagger_{\mathbf{k}}, d^\dagger_{\mathbf{k}} \right) \mathsf{H}_{NNN}(\mathbf{k}) \begin{pmatrix} c_{\mathbf{k}} \\ d_{\mathbf{k}} \end{pmatrix} && (1.71)
\end{aligned}$$

where

$$\mathsf{H}_{NNN}(\mathbf{k}) = 2t_2 \begin{pmatrix} \sum_i \cos(\mathbf{k}\cdot\mathbf{a}_i + \phi) & 0 \\ 0 & \sum_i \cos(\mathbf{k}\cdot\mathbf{a}_i - \phi) \end{pmatrix}. \tag{1.72}$$

After including the $\hat{H}_{NN}$ and $\hat{H}_{on-site}$ obtained earlier, the total Hamiltonian can be written as

$$\mathsf{H}(\mathbf{k}) = \frac{h_{11} + h_{22}}{2} + \mathbf{h}\cdot\boldsymbol{\sigma}, \tag{1.73}$$

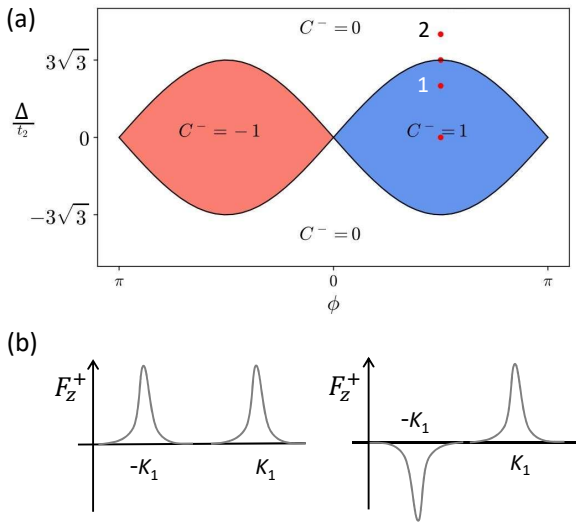

FIG. 6 (a) The quantum phases of the Haldane model. Fig. from J. Atteia's thesis, 2018. (b) Schematic plots of the Berry curvatures for point-1 in (a)-left, and point-2 in (a)-right.

in which h_{11}, h_{22} are the diagonal matrix elements of H_{NNN}, and

$$\mathbf{h} = \left(t_1 \sum_i \cos \mathbf{k}\cdot\boldsymbol{\delta}_i, -t_1 \sum_i \sin \mathbf{k}\cdot\boldsymbol{\delta}_i, \frac{h_{11}-h_{22}}{2} + \Delta \right). \tag{1.74}$$

The third component of $\mathbf{h}$,

$$h_3(\mathbf{k}) = \frac{h_{11}-h_{22}}{2} + \Delta \tag{1.75}$$

$$= -2t_2 \sum_i \sin \mathbf{k}\cdot\mathbf{a}_i \sin\phi + \Delta. \tag{1.76}$$

It can be shown that, near $\mathbf{K}_1$ and $-\mathbf{K}_1$,

$$h_3(\mathbf{k}) = \pm 3\sqrt{3}t_2 \sin\phi + \Delta + O(k^2). \tag{1.77}$$

This can be considered as a flux-dependent (and valley-dependent) Dirac mass $h_3 = m_\tau(\phi, \Delta)$, such that near $\tau\mathbf{K}(\tau = \pm)$,

$$\mathsf{H}_\tau(\mathbf{k}) = \frac{h_{11}+h_{22}}{2} + \begin{pmatrix} m_\tau & \hbar v_F(\tau k_x - i k_y) \\ \hbar v_F(\tau k_x + i k_y) & -m_\tau \end{pmatrix}. \tag{1.78}$$

2. Berry curvature

From Eq. (1.51), the Berry curvatures for conduction band near the Dirac points are

$$F_{z\tau}^+(\mathbf{k}) = \frac{\tau}{2} \frac{\hbar^2 v_F^2 m_\tau}{\left(\hbar^2 v_F^2 k^2 + m_\tau^2\right)^{3/2}}. \tag{1.79}$$

The energy gap is closed when

$$m_\pm(\phi, \Delta) = \pm 3\sqrt{3}t_2 \sin\phi + \Delta = 0. \tag{1.80}$$

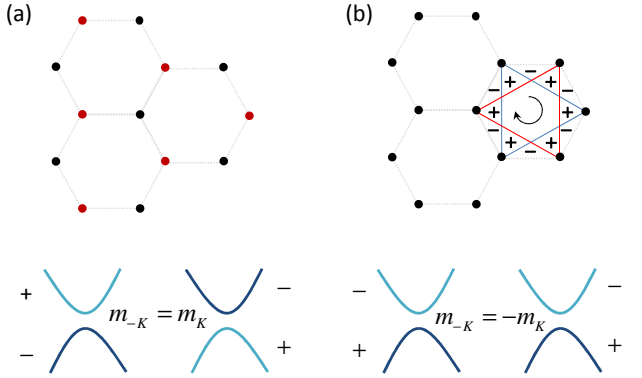

FIG. 7 (a) Graphene lattice with staggered on-site potentials opens a gap at a Dirac point, which is described by a mass. (b) A special distribution of magnetic flux invented by Haldane also opens a gap at a Dirac point, which is described by a valley-dependent mass.

Depending on the parameters Δ, ϕ, the effective mass can be positive or negative, which leads to different topological phases (see Fig. 6). For example, when $\phi = 0$, then $m_\pm = \Delta$ and the Berry curvatures $F_{z\pm}^+$ at $\pm\mathbf{K}_1$ have opposite signs. The Chern number of a filled band is zero and the insulator phase is trivial .

On the other hand, when $\Delta = 0$, then $m_\pm$ have opposite signs at $\pm\mathbf{K}_1$, so that the Berry curvatures $F_{z\pm}^+$ have the same sign at two Dirac points (whether this sign is positive or negative is dependent on the direction of flux ϕ). As a result, the Chern number of a filled band is nonzero and the insulator phase has nontrivial topology. Suppose $\phi > 0$, and $\Delta(> 0)$ is turned on from zero, then the system remains topological when $\Delta < 3\sqrt{3}t_2 \sin\phi$, until the energy gap at $-\mathbf{K}_1$ closes ($m_- = 0$). Such a closure flips the signs of the Berry curvatures of the conduction band and the valence band at $-\mathbf{K}_1$, and the systems enters the trivial phase. Fig. 7 is a comparison of the Berry curvatures between the usual graphene and the graphene with Haldane flux.

Two remarks about Haldane's graphene model: First, with proper tuning of model parameters, it's possible *not* to open the two nodes simultaneously. That is, there can be only one Dirac point, not two, at critical values. This demonstrates the **parity anomaly** in (2+1)-dimensional field theories.

C. Transition Metal Dichalcogenide

Transition metal dichalcogenide (TMD) is a class of chemical compound containing transition metals and chalcogens. Chalcogen refers to group-16 elements such as oxygen O, sulfur S, selenium Se, and tellurium Te. The chemical formula of TMD is MX_2, where M is a transition metal atom, and X a chalcogen atom. TMD could form layered structure similar to the graphene lay-

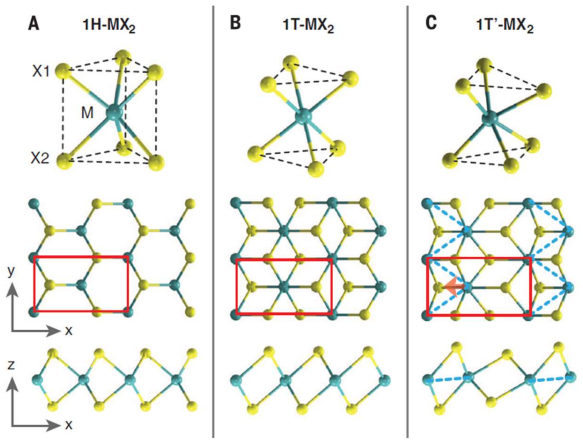

FIG. 8 The 1H, 1T, and 1T' structures of monolayer MX_2. Fig. from Qian *et al.*, 2014.

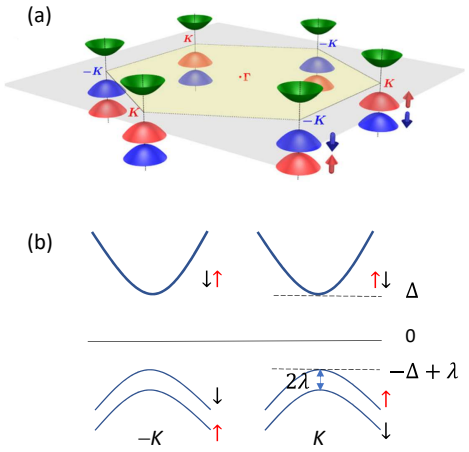

FIG. 9 (a) Conduction and valence bands near the Dirac points. Fig. from Xiao *et al.*, 2012. (b) The valence bands are gapped by spin-orbit coupling (and the breaking of space-inversion symmetry), while the conduction bands have little SO-splitting. Time-reversal symmetry requires the spins to be opposite at opposite valleys.

ers. Both graphene and layered TMD belong to a larger class of layered materials called **van de Waals materials** (which also include h-BN, black phosphorous, CrI_3 etc), because of the van der Waals binding force between these layers. They provide a major playground for various exciting physics of two-dimensional electrons.

Several TMDs could be stable as a monolayer. For exmaple, the compounds of
Group IV: Ti, Zr, Hf
Group V: V, Nb, Ta with S, Se, Te.
Group VI: Mo, W.
We'll focus on group-VI compounds that have observed topological phases. One monolayer of these TMDs may have one of the structures shown in Fig. 8:
Trigonal prismatic structure (1H),
Octahedral structure (1T), or
Distorted octahedral structure (1T').
The distorted sructure 1T' is more stable than 1T. Note that a monolayer under strain could transit to a different structure.

Let's focus on one of the group-VI compounds: MoS_2. It has indirect band gap for bulk material, but direct band gap (about 1.9 eV) for a monolayer. Similar to graphene, a MoS_2 monolayer has a hexagonal Brillouin zone, with Dirac points at corners (Fig. 9). What is different is that in a TMD,
1. There is no inversion symmetry, so that the Dirac points are gapped.
2. There is a large spin-orbit (SO) coupling due to the d-orbitals of the transition metal atoms. This results in spin-valley locking, which is favourable for spintronics applications.

To first order in k, a 4-band Hamiltonian near the Dirac points can be written as $H_{4\times4} = H_0 + H_{SO}$ (Xiao *et al.*, 2012), where

$$H_0 = \alpha(\tau k_x\sigma_x + k_y\sigma_y) + \Delta\sigma_z \tag{1.81}$$
$$H_{SO} = -\lambda\tau\frac{\sigma_z - 1}{2}s_z, \tag{1.82}$$

in which $\tau = \pm$ for $\pm K$-valley, $\boldsymbol{\sigma}$ refers to the quasi-spin of sublattices, and s_z relates to electron spin. The SO-gap of the valence bands is given by $2\lambda \simeq 0.2$ eV. Suppose only the conduction band and the upper valence band ($\tau s_z = +1$) are active, then we can ignore the lower valence band and study the 2-band Hamiltonian,

$$H = \alpha(\tau k_x\sigma_x + k_y\sigma_y) + \Delta'\sigma_z + \frac{\lambda}{2}, \tag{1.83}$$

where $\Delta' \equiv \Delta - \lambda/2$. The band energies near the Dirac points are

$$\varepsilon_k^{c/v} = \pm\sqrt{\alpha^2k^2 + \Delta'^2} + \frac{\lambda}{2}. \tag{1.84}$$

The last term in H contributes to a constant energy shift that does not affect the Berry curvature.

1. Berry curvature

Based on earlier calculations such as Eq. 1.51, we know that the Berry curvature of the conduction band would be

$$F_c^\tau(\mathbf{k}) = \frac{\tau}{2}\frac{\alpha^2\Delta'}{\left[\alpha^2k^2 + \Delta'^2\right]^{3/2}}. \tag{1.85}$$

On the other hand, the Berry curvature for the valence band $F_v^\tau(\mathbf{k}) = -F_c^\tau(\mathbf{k})$.

For one valley in a partially-filled *conduction band*, the Berry curvature contributes to the Hall conductivity (in units of e^2/h),

$$\sigma_H^\tau = \frac{1}{2\pi}\int d^2k F_c^\tau(\mathbf{k}) \tag{1.86}$$

$$= \frac{\tau}{2}\left[1 - \frac{\Delta'}{\sqrt{\alpha^2 k_F^2 + \Delta'^2}}\right]. \tag{1.87}$$

Suppose the chemical potential is measured from the bottom of the conduction band, then

$$\mu = \varepsilon^c_{k_F} - \Delta. \tag{1.88}$$

That is, $\mu = 0$ when $k_F = 0$. The Hall conductivity can be written as

$$\sigma_H^\tau = \frac{\tau}{2}\left(1 - \frac{\Delta - \frac{\lambda}{2}}{\mu + \Delta - \frac{\lambda}{2}}\right) \tag{1.89}$$

$$= \frac{\tau}{2}\frac{\mu}{\mu + \Delta - \frac{\lambda}{2}}. \tag{1.90}$$

The sum of the Hall conductivities from two valleys is zero.

On the other hand, for partially-filled upper *valence band*, suppose the chemical potential is measured from the top of the valence band, then

$$\mu = \varepsilon^v_{k_F} - (-\Delta + \lambda). \tag{1.91}$$

The Hall conductivity

$$\sigma_H^\tau = \frac{1}{2\pi}\int d^2k F_v^\tau(\mathbf{k}) \tag{1.92}$$

$$= -\frac{\tau}{2}\left[1 - \frac{\Delta'}{\sqrt{\alpha^2 k_F^2 + \Delta'^2}}\right] \tag{1.93}$$

$$= -\frac{\tau}{2}\frac{\mu}{\mu - \Delta + \frac{\lambda}{2}}. \tag{1.94}$$

Again the sum of the Hall conductivities from two valleys is zero.

In order to have a non-zero Hall conductivity, the populations of the electrons (or holes) in two valleys need be different. Assume the chemical potentials of electrons in $\pm K$ valley are $\mu_{\pm K}$, and $\Delta\mu = \mu_K - \mu_{-K}$. Suppose $\mu_{\pm K}$ are much smaller than the energy gap $\varepsilon_g = 2\Delta - \lambda$, then the total Hall conductivity

$$\sigma_H = \sigma_H^+ + \sigma_H^- \tag{1.95}$$

$$\simeq \frac{\Delta\mu}{2\Delta - \lambda} = \frac{\Delta\mu}{\varepsilon_g}. \tag{1.96}$$

For a two-dimensional system, $\mu = (\hbar^2/2m)2\pi n$, where n is the electron density. Therefore (putting e^2/h back),

$$\sigma_H \simeq \left(\frac{e^2}{h}\right)\frac{\hbar^2}{m}\frac{\pi\Delta n}{\varepsilon_g} = \frac{e^2\hbar}{2m}\frac{\Delta n}{\varepsilon_g}. \tag{1.97}$$

This is called the **valley Hall effect**.

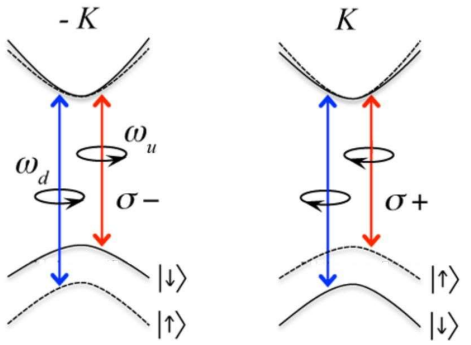

FIG. 10 Optical transitions induced by circularly polarized light. Fig. from Xiao *et al.*, 2012.

2. Optical transitions

One can use circularly-polarized light to pump electrons to a preferred valley. Write the matrix element of momentum operator as $\mathcal{P}_\ell(\mathbf{k}) \equiv \langle\psi_c|p_\ell|\psi_v\rangle$ ($\ell = x, y$). The transition probabilities due to $\sigma_\pm$ circularly-polarized light are proportional to $\mathcal{P}_\pm = |\mathcal{P}_x \pm i\mathcal{P}_y|^2$.

The effective Hamiltonian near Dirac points are

$$\mathsf{H}(\mathbf{k}) = \begin{pmatrix} \Delta' & \alpha(\tau k_x - i k_y) \\ \alpha(\tau k_x + i k_y) & -\Delta' \end{pmatrix}, \tag{1.98}$$

with the eigenstates

$$u_c = N\begin{pmatrix} \Delta' + \sqrt{} \\ \alpha(\tau k_x + i k_y) \end{pmatrix},\ u_v = N\begin{pmatrix} -\alpha(\tau k_x - i k_y) \\ \Delta' + \sqrt{} \end{pmatrix}, \tag{1.99}$$

where

$$\sqrt{} \equiv \sqrt{\alpha^2 k^2 + \Delta'^2}, \tag{1.100}$$

$$\text{and}\quad N \equiv \left[2\sqrt{}\left(\sqrt{} + \Delta'\right)\right]^{-1/2}. \tag{1.101}$$

It is known that

$$\langle\psi_c|\mathbf{p}|\psi_v\rangle \Rightarrow \frac{m}{\hbar}\langle u_c|\frac{\partial\mathsf{H}(\mathbf{k})}{\partial\mathbf{k}}|u_v\rangle, \tag{1.102}$$

and

$$\frac{\partial\mathsf{H}(\mathbf{k})}{\partial k_x} = \alpha\tau\sigma_x,\quad \frac{\partial\mathsf{H}(\mathbf{y})}{\partial k_y} = \alpha\sigma_y. \tag{1.103}$$

After some calculations, we have

$$\mathcal{P}_\pm(\mathbf{k}) = \alpha^2\left(1 \pm \tau\frac{\Delta'}{\sqrt{\alpha^2 k^2 + \Delta'^2}}\right)^2. \tag{1.104}$$

The carriers near K-valley and K'-valley respond differently to right (or left) circularly-polarized light. Pump different amount of electrons to two valleys so that $\Delta\mu \neq 0$, one can then detect the valley Hall effect given in Eq. 1.97 (Mak *et al.*, 2014).

D. Twisted bilayer graphene

Suppose there are two overlapped graphene sheets, and layer-1 is on top of layer-2. Layer-1 (layer-2) is rotated clockwise (counter-clockwise) with a small angle $\theta/2$. These two sheets with slightly different orientations would visually form an interference pattern called the Moiré pattern, as shown in Fig. 11(a). The Moiré pattern has a pattern of a superlattice with hexagonal symmetry. Upon closer look, there are 3 different types of stacking, AA, AB, and BA near symmetry points. That is, A-site on top of A-site, A-site on top of B-site etc. When the angular difference θ between two sheets is small, the distance between two neighboring AA sites

$$L = \frac{a}{2\sin\frac{\theta}{2}}. \tag{1.105}$$

Note: Rigorously speaking, there is a periodic superlattice only when the positions of the two graphene layers are commensurate. However, even if not, a non-commensurate overlap would produce a Moiré pattern with similar electronic property to a commensurate one nearby. Hence we will ignore such a quasi-periodicity.

This superlattice has a corresponding mini-BZ, as shown in Fig. 11(b). If K_D is the distance between two neighboring Dirac points of a graphene sheet, then the scale of the mini-BZ

$$k_\theta = 2K_D \sin\frac{\theta}{2}. \tag{1.106}$$

In reality, two graphene sheets are known to be separated by $\Delta z \simeq 2.35\mathring{A}$. Furthermore, there is a slight undulation in the graphene sheets. The vertical separation for the AB stacking is smaller than the AA stacking by about $0.15\mathring{A}$.

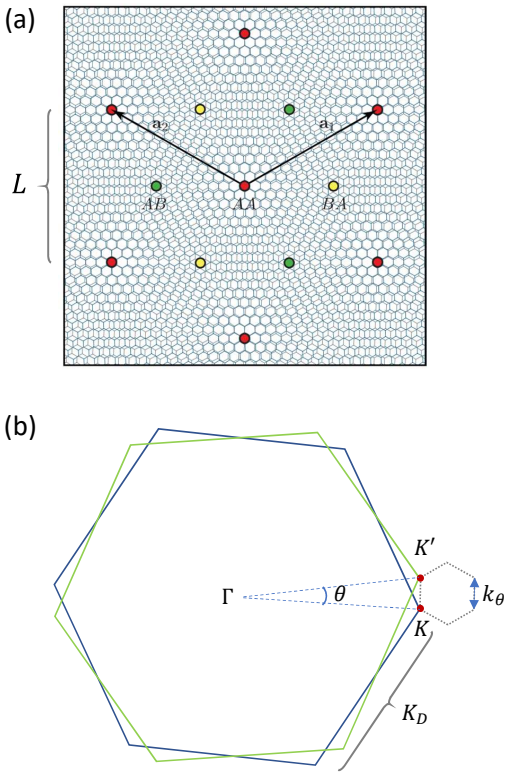

FIG. 11 (a) The Moiré pattern of twisted bilayer graphene. Fig. from Ledwith *et al.*, 2021. (b) The rotated Brillouin zones of twisted bilayer graphene.

1. Tight-binding model

The carbon atoms in layer-1 are located at

$$\mathbf{R}_\alpha = n_1\mathbf{a}_1 + n_2\mathbf{a}_2 + \boldsymbol{\delta}_\alpha \tag{1.107}$$
$$= \mathbf{R} + \boldsymbol{\delta}_\alpha,\ \alpha = A, B \tag{1.108}$$

in which $\boldsymbol{\delta}_A = 0$, and $\boldsymbol{\delta}_B = \boldsymbol{\delta}$ is a displacement of a B-site with respect to a neighboring A-site. The carbon atoms in layer-2 are located at

$$\mathbf{R}'_\beta = \mathbf{R}' + \boldsymbol{\delta}'_\beta + \mathbf{d},\ \beta = A, B \tag{1.109}$$
$$= \mathsf{M}\left(\mathbf{R} + \boldsymbol{\delta}_\beta\right) + \mathbf{d}, \tag{1.110}$$

where M is a rotation matrix, and $\mathbf{d}$ is a general displacement between two layers.

The Hamiltonian has three parts,

$$\hat{H} = \hat{H}_1 + \hat{H}_2 + \hat{H}_{12}, \tag{1.111}$$

in which $\hat{H}_1$ and $\hat{H}_2$ are the Hamiltonians for layer-1 and layer-2. $\hat{H}_{12}$ describes the coupling between two layers,

$$\hat{H}_{12} = \sum_{\mathbf{R},\mathbf{R}'}\sum_{\alpha,\beta} t_\perp\left(\mathbf{R}_\alpha - \mathbf{R}'_\beta\right) c^\dagger(\mathbf{R}_\alpha)c(\mathbf{R}'_\beta) + h.c. \tag{1.112}$$

The positions for layer-2 are distinguished from those of layer-1 by having 'primes' in their arguments.

We'll rely on the Fourier transformations,

$$c(\mathbf{R}_\alpha) = \frac{1}{\sqrt{N}}\sum_{\mathbf{k}} e^{i\mathbf{k}\cdot\mathbf{R}_\alpha} c_{\alpha\mathbf{k}}, \tag{1.113}$$
$$c(\mathbf{R}'_\beta) = \frac{1}{\sqrt{N}}\sum_{\mathbf{k}'} e^{i\mathbf{k}'\cdot\mathbf{R}'_\beta} c_{\beta\mathbf{k}'}. \tag{1.114}$$

The tunnelling amplitudes $t_\perp\left(\mathbf{R}_\alpha - \mathbf{R}'_\beta\right)$ have a triangular pattern for each pair of (α, β) (see Fig. 11(a)), hence we can decompose

$$t_\perp\left(\mathbf{R}_\alpha - \mathbf{R}'_\beta\right) = \frac{1}{N}\sum_{\mathbf{q}} t_\perp^{\alpha\beta}(\mathbf{q}) e^{i\mathbf{q}\cdot\left(\mathbf{R}_\alpha - \mathbf{R}'_\beta\right)},$$
$$\text{conversely, } t_\perp^{\alpha\beta}(\mathbf{q}) = \sum_{\mathbf{R}_\alpha} t_\perp(\mathbf{R}_\alpha - \mathbf{R}'_\beta) e^{-i\mathbf{q}\cdot\left(\mathbf{R}_\alpha - \mathbf{R}'_\beta\right)}.$$

It follows that

$$\begin{aligned}&\hat{H}_{12}\\ &= \frac{1}{N}\sum_{\mathbf{k},\mathbf{k}'}\sum_{\alpha,\beta}\sum_{\mathbf{R},\mathbf{R}'} t_\perp(\mathbf{R}_\alpha-\mathbf{R}'_\beta)e^{-i\mathbf{k}\cdot\mathbf{R}_\alpha+i\mathbf{k}'\cdot\mathbf{R}'_\beta}c^\dagger_{\alpha\mathbf{k}}c_{\beta\mathbf{k}'}+h.c.\\ &= \sum_{\mathbf{k},\mathbf{k}'}\sum_{\alpha,\beta}\left(T^{\alpha\beta}_{\mathbf{k}\mathbf{k}'}c^\dagger_{\alpha\mathbf{k}}c_{\beta\mathbf{k}'}+T^{\beta\alpha}_{\mathbf{k}'\mathbf{k}}c^\dagger_{\beta\mathbf{k}'}c_{\alpha\mathbf{k}}\right),\end{aligned} \tag{1.115}$$

in which

$$T^{\alpha\beta}_{\mathbf{k}\mathbf{k}'}\equiv\frac{1}{N^2}\sum_{\mathbf{R},\mathbf{R}'}\sum_{\mathbf{q}}t^{\alpha\beta}_\perp(\mathbf{q})e^{i\mathbf{q}\cdot(\mathbf{R}_\alpha-\mathbf{R}'_\beta)}e^{-i\mathbf{k}\cdot\mathbf{R}_\alpha+i\mathbf{k}'\cdot\mathbf{R}'_\beta}. \tag{1.116}$$

Write $\mathbf{R}_\alpha$, $\mathbf{R}'_\beta$ in terms of $\mathbf{R}$, $\mathbf{R}'$, as shown in Eqs. (1.108) and (1.109). Carry out the summation over $\mathbf{R}$, $\mathbf{R}'$ using the orthogonality relations,

$$\sum_{\mathbf{R}}e^{-i(\mathbf{k}-\mathbf{q})\cdot\mathbf{R}} = N\sum_{\mathbf{G}}\delta_{\mathbf{k}-\mathbf{q},\mathbf{G}}, \tag{1.117}$$

$$\sum_{\mathbf{R}'}e^{i(\mathbf{k}'-\mathbf{q})\cdot\mathbf{R}'} = N\sum_{\mathbf{G}}\delta_{\mathbf{k}'-\mathbf{q},\mathbf{G}'}, \tag{1.118}$$

in which $\mathbf{G}$, $\mathbf{G}'$ are reciprocal lattice vectors for layer-1 and -2 respectively. This leads to

$$T^{\alpha\beta}_{\mathbf{k}\mathbf{k}'}=\sum_{\mathbf{G},\mathbf{G}'}t^{\alpha\beta}_\perp(\mathbf{k}-\mathbf{G})e^{-i\mathbf{G}\cdot\boldsymbol{\delta}_\alpha}e^{+i\mathbf{G}'\cdot(\boldsymbol{\delta}'_\beta+\mathbf{d})}\delta_{\mathbf{k}-\mathbf{G},\mathbf{k}'-\mathbf{G}'}. \tag{1.119}$$

The delta function gives the rule for momentum conservation,

$$\mathbf{k}'-\mathbf{G}'=\mathbf{k}-\mathbf{G}. \tag{1.120}$$

For example, if $\mathbf{k}$ is located at the $\mathbf{K}$-valley, then it could couple with $\mathbf{k}'$ at the $\mathbf{K}'$-valley (call it Q_0) and the other two valleys Q_1, Q_2 via $\mathbf{G}'_1-\mathbf{G}_1$ and $\mathbf{G}_2-\mathbf{G}'_2$ (Fig. 12(a)), where

$$\mathbf{G}_1 = \frac{2\pi}{a}\left(+\frac{1}{\sqrt{3}}\hat{x}+\frac{1}{3}\hat{y}\right), \tag{1.121}$$

$$\mathbf{G}_2 = \frac{2\pi}{a}\left(-\frac{1}{\sqrt{3}}\hat{x}+\frac{1}{3}\hat{y}\right), \tag{1.122}$$

$$\text{and } \mathbf{G}_3 = -\frac{2\pi}{a}\frac{2}{3}\hat{y}. \tag{1.123}$$

As a result,

$$\begin{aligned}\hat{H}_{12} &= \sum_{\mathbf{k},\mathbf{k}'}\sum_{\alpha,\beta}\Big[t^{\alpha\beta}_\perp(Q_0)\delta_{\mathbf{k},\mathbf{k}'}\\ &+ t^{\alpha\beta}_\perp(Q_1)e^{-i\mathbf{G}_1\cdot\boldsymbol{\delta}_\alpha}e^{+i\mathbf{G}'_1\cdot(\boldsymbol{\delta}'_\beta+\mathbf{d})}\delta_{\mathbf{k}-\mathbf{G}_1,\mathbf{k}'-\mathbf{G}'_1}\\ &+ t^{\alpha\beta}_\perp(Q_2)e^{+i\mathbf{G}_2\cdot\boldsymbol{\delta}_\alpha}e^{-i\mathbf{G}'_2\cdot(\boldsymbol{\delta}'_\beta+\mathbf{d})}\delta_{\mathbf{k}+\mathbf{G}_2,\mathbf{k}'+\mathbf{G}'_2}\Big]\\ &\times c^\dagger_{\alpha\mathbf{k}}c_{\beta\mathbf{k}'}+h.c.\end{aligned} \tag{1.124}$$

According to Eq. (1.115), the square bracket $[\ ]=T^{\alpha\beta}_{\mathbf{k}\mathbf{k}'}$, which has the form

$$\begin{aligned}T^{\alpha\beta}_{\mathbf{k}\mathbf{k}'} &= T_{\alpha\beta}(Q_0)\delta_{\mathbf{k},\mathbf{k}'}+T_{\alpha\beta}(Q_1)\delta_{\mathbf{k}-\mathbf{G}_1,\mathbf{k}'-\mathbf{G}'_1}\\ &+ T_{\alpha\beta}(Q_2)\delta_{\mathbf{k}+\mathbf{G}_2,\mathbf{k}'+\mathbf{G}'_2},\end{aligned} \tag{1.125}$$

in which $T_{\alpha\beta}(Q_\ell)$ are the factors multiplying the delta functions. When being written in matrices, we have

$$\begin{aligned}\mathsf{T}_{\mathbf{k}\mathbf{k}'} &= \mathsf{T}(Q_0)\delta_{\mathbf{k},\mathbf{k}'}+\mathsf{T}(Q_1)\delta_{\mathbf{k}-\mathbf{G}_1,\mathbf{k}'-\mathbf{G}'_1}\\ &+ \mathsf{T}(Q_2)\delta_{\mathbf{k}+\mathbf{G}_2,\mathbf{k}'+\mathbf{G}'_2}.\end{aligned} \tag{1.126}$$

For the exponents in Eq. (1.124), we have $\mathbf{G}'\cdot\boldsymbol{\delta}'_\beta=\mathbf{G}\cdot\boldsymbol{\delta}_\beta$, and

$$\mathbf{G}\cdot\boldsymbol{\delta}_\alpha-\mathbf{G}'\cdot\boldsymbol{\delta}'_\beta=\mathbf{G}\cdot(\boldsymbol{\delta}_\alpha-\boldsymbol{\delta}_\beta). \tag{1.127}$$

Depending on whether the stacking is AA, AB, or BA, the difference $\boldsymbol{\delta}_\alpha-\boldsymbol{\delta}_\beta$ can be $0, -\boldsymbol{\delta}$, or $+\boldsymbol{\delta}$. We can choose the displacement $\boldsymbol{\delta}=-a\hat{y}$ (see Eq. (1.9)), such that

$e^{i\mathbf{G}_i\cdot(\boldsymbol{\delta}_\alpha-\boldsymbol{\delta}_\beta)}$	AA	AB	BA
$\mathbf{G}_1$	1	$e^{-\frac{2\pi}{3}i}$	$e^{+\frac{2\pi}{3}i}$
$\mathbf{G}_2$	1	$e^{-\frac{2\pi}{3}i}$	$e^{+\frac{2\pi}{3}i}$

(1.128)

It follows that, if we write

$$t\equiv t^{AB}_\perp(Q_\ell),\quad \gamma\equiv\frac{t^{AA}_\perp}{t^{AB}_\perp}, \tag{1.129}$$

then

$$\mathsf{T}(Q_0) = t\begin{pmatrix}\gamma & 1\\ 1 & \gamma\end{pmatrix}, \tag{1.130}$$

$$\mathsf{T}(Q_1) = t\begin{pmatrix}\gamma & e^{i2\pi/3}\\ e^{-i2\pi/3} & \gamma\end{pmatrix}e^{+i\mathbf{G}'_1\cdot\mathbf{d}}, \tag{1.131}$$

$$\mathsf{T}(Q_2) = t\begin{pmatrix}\gamma & e^{-i2\pi/3}\\ e^{i2\pi/3} & \gamma\end{pmatrix}e^{-i\mathbf{G}'_2\cdot\mathbf{d}}. \tag{1.132}$$

When $\theta=0$, Bernard (AB) stacking is preferred. Thus AB stacking has a larger tunnelling amplitude compared to AA stacking, and γ is estimated to be $0.7\sim0.8$.

Finally, the low-energy Hamiltonian near a Dirac point is,

$$\begin{aligned}\hat{H} &= \hat{H}_1+\hat{H}_2+\hat{H}_{12}\\ &= \sum_{\mathbf{k}}\psi^\dagger_{1\mathbf{k}}\hbar v_F\boldsymbol{\sigma}^{-\frac{\theta}{2}}\cdot(\mathbf{k}-\mathbf{K})\psi_{1\mathbf{k}}\\ &+ \sum_{\mathbf{k}'}\psi^\dagger_{2\mathbf{k}'}\hbar v_F\boldsymbol{\sigma}^{+\frac{\theta}{2}}\cdot(\mathbf{k}'-\mathbf{K}')\psi_{2\mathbf{k}'}\\ &+ \sum_{\mathbf{k},\mathbf{k}'}\left(\psi^\dagger_{1\mathbf{k}},\psi^\dagger_{2\mathbf{k}'}\right)\begin{pmatrix}0 & \mathsf{T}_{\mathbf{k}\mathbf{k}'}\\ \mathsf{T}^\dagger_{\mathbf{k}'\mathbf{k}} & 0\end{pmatrix}\begin{pmatrix}\psi_{1\mathbf{k}}\\ \psi_{2\mathbf{k}'}\end{pmatrix},\end{aligned} \tag{1.133}$$

in which

$$\boldsymbol{\sigma}^{\pm\frac{\theta}{2}}\equiv U^\dagger\left(\pm\frac{\theta}{2}\right)\boldsymbol{\sigma}U\left(\pm\frac{\theta}{2}\right),\ U(\phi)=e^{-i\frac{\phi}{2}\sigma_z} \tag{1.134}$$

and $(\psi_{1\mathbf{k}},\psi_{2\mathbf{k}'})^T=(c_{1A\mathbf{k}},c_{1B\mathbf{k}},c_{2A\mathbf{k}'},c_{2B\mathbf{k}'})^T$.

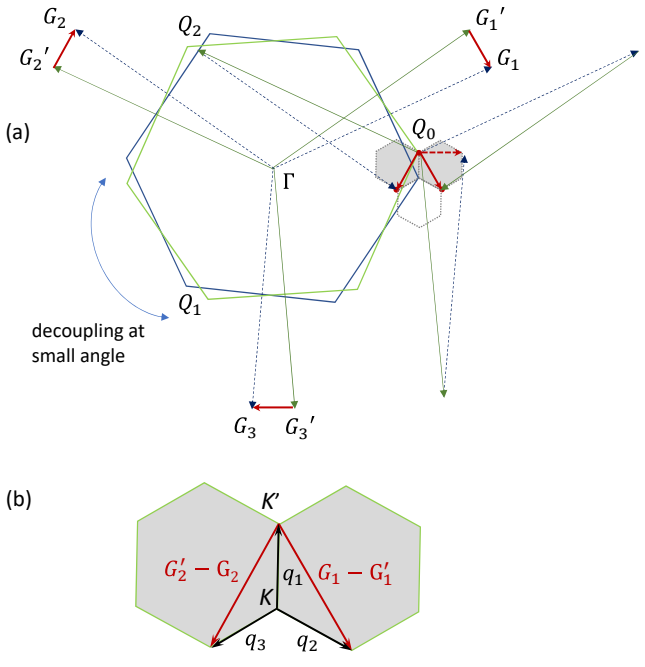

FIG. 12 (a) The valleys Q_0, Q_1, Q_2 could couple with each other with the conservation of momentum $\mathbf{k} = \mathbf{k}' + \mathbf{G}_i' - \mathbf{G}_i$. (b) Some vectors in the mini-BZ.

The Schrödinger equation in momentum space would be

$$\begin{pmatrix} \hbar v_F \boldsymbol{\sigma}^{-\frac{\theta}{2}} \cdot (\mathbf{k} - \mathbf{K}) & \mathsf{T}_{\mathbf{k}\mathbf{k}'} \\ \mathsf{T}^{\dagger}_{\mathbf{k}'\mathbf{k}} & \hbar v_F \boldsymbol{\sigma}^{+\frac{\theta}{2}} \cdot (\mathbf{k}' - \mathbf{K}') \end{pmatrix} \begin{pmatrix} \psi_1(\mathbf{k}) \\ \psi_2(\mathbf{k}') \end{pmatrix} = \varepsilon \begin{pmatrix} \psi_1(\mathbf{k}) \\ \psi_2(\mathbf{k}') \end{pmatrix}, \quad (1.135)$$

in which the column vectors are state functions, instead of annihilation operators.

Exercise

1. The effective two-band Hamiltonian for graphene with *gapped* Dirac points is

$$\mathsf{H}_0 = \hbar v_F \left(\pm k_x \sigma_x + k_y \sigma_y\right) + \Delta \sigma_z, \text{ near } \pm K, \quad (1.136)$$

where v_F is the Fermi velocity, $\boldsymbol{\sigma}$ is the quasi-spin for orbital degrees of freedom (i.e., conduction and valence bands), and $\pm K$ are the indices for two Dirac valleys.
(a) Using Eq. (1.49), show that the Berry curvatures $F_{z\tau}^{\pm K}$ are given by Eq. (1.51).
(b) What would the Berry curvatures become if the Dirac points are gapless (i.e. $\Delta = 0$)?

2. Starting from Eq. (1.49), show that the Berry curvature of graphene is given as Eq. (1.50).

3. (a) Given the Hamiltonian in Eq. 1.98 and the eigenstates in Eq. 1.99, show that the Berry connections are,

$$A_x^{\pm}(\mathbf{k}) = \frac{\tau}{2}\left(1 - \frac{\Delta'}{\sqrt{\ }}\right)\frac{(\pm k_y)}{k^2}, \quad (1.137)$$

$$A_y^{\pm}(\mathbf{k}) = \frac{\tau}{2}\left(1 - \frac{\Delta'}{\sqrt{\ }}\right)\frac{(\mp k_x)}{k^2}. \quad (1.138)$$

(b) Verify that the eigenstates can also be

$$u^{+} = N'\begin{pmatrix} \Delta' + \sqrt{\ } \\ \alpha(\tau k_x + i k_y) \end{pmatrix}, \; u^{-} = N'\begin{pmatrix} \Delta' - \sqrt{\ } \\ \alpha(\tau k_x + i k_y) \end{pmatrix},$$

where $N' \equiv [2\sqrt{\ }(\sqrt{\ } - \Delta')]^{-1/2}$. Show that the Berry connections are

$$A_x^{\pm}(\mathbf{k}) = \frac{\tau}{2}\left(1 \mp \frac{\Delta'}{\sqrt{\ }}\right)\frac{(+k_y)}{k^2}, \quad (1.139)$$

$$A_y^{\pm}(\mathbf{k}) = \frac{\tau}{2}\left(1 \mp \frac{\Delta'}{\sqrt{\ }}\right)\frac{(-k_x)}{k^2}, \quad (1.140)$$

which are different from the result in (a). Why this answer makes no sense in physics?

REFERENCES

Cayssol, J, and J N Fuchs (2021), "Topological and geometrical aspects of band theory," Journal of Physics: Materials **4** (3), 034007.

Chang, Ming-Che, and Qian Niu (1996), "Berry phase, hyperorbits, and the hofstadter spectrum: Semiclassical dynamics in magnetic bloch bands," Phys. Rev. B **53**, 7010–7023.

Duca, L, T. Li, M. Reitter, I. Bloch, M. Schleier-Smith, and U. Schneider (2015), "An aharonov-bohm interferometer for determining bloch band topology," **347** (6219), 288–292.

Haldane, F D M (1988), "Model for a quantum hall effect without landau levels: Condensed-matter realization of the "parity anomaly"," Phys. Rev. Lett. **61**, 2015–2018.

He, Hong-Tao, Gan Wang, Tao Zhang, Iam-Keong Sou, George K. L Wong, Jian-Nong Wang, Hai-Zhou Lu, Shun-Qing Shen, and Fu-Chun Zhang (2011), "Impurity effect on weak antilocalization in the topological insulator bi_2te_3," Phys. Rev. Lett. **106**, 166805.

Ledwith, Patrick J, Eslam Khalaf, and Ashvin Vishwanath (2021), "Strong coupling theory of magic-angle graphene: A pedagogical introduction," Annals of Physics **435**, 168646, special issue on Philip W. Anderson.

Lu, Hai-Zhou, and Shun-Qing Shen (2014), "Weak localization and weak anti-localization in topological insulators," Proc.SPIE **9167**, 9167.

Mak, K F, K. L. McGill, J. Park, and P. L. McEuen (2014), "The valley hall effect in mos2 transistors," Science **344** (6191), 1489–1492.

Qian, Xiaofeng, Junwei Liu, Liang Fu, and Ju Li (2014), "Quantum spin hall effect in two-dimensional transition metal dichalcogenides," Science **346** (6215), 1344–1347.

Tikhonenko, F V, A. A. Kozikov, A. K. Savchenko, and R. V. Gorbachev (2009), "Transition between electron localization and antilocalization in graphene," Phys. Rev. Lett. **103**, 226801.

Xiao, Di, Ming-Che Chang, and Qian Niu (2010), "Berry phase effects on electronic properties," Rev. Mod. Phys. **82**, 1959–2007.

Xiao, Di, Gui-Bin Liu, Wanxiang Feng, Xiaodong Xu, and Wang Yao (2012), "Coupled spin and valley physics in monolayers of mos_2 and other group-vi dichalcogenides," Phys. Rev. Lett. **108**, 196802.